IEEE Access
Multidisciplinary ⋮ Rapid Review ⋮ Open Access Journal

Received 29 September 2024, accepted 12 December 2024, date of publication 4 March 2025, date of current version 24 March 2025.

Digital Object Identifier 10.1109/ACCESS.2025.3547711

RESEARCH ARTICLE

Cancer Cell Classification Based on Morphological Features of 3D Phase Contrast Microscopy Using Deep Neural Network

MISUN KANG[1] **AND JUNGYOON KIM**[2]
[1]Department of Applied Artificial Intelligence, Hansung University, Seoul 02876, Republic of Korea
[2]Department of Computer Science, Kent State University, Kent, OH 44242, USA

Corresponding author: Jungyoon Kim (jkim78@kent.edu)

This research was financially supported by Hansung University.

ABSTRACT 3D phase contrast microscopy is one of the most common imaging modalities for the observation of long-term multicellular processes of living cells without phototoxicity and photobleaching, because the morphological features of cancer cells can be used as an indicator of metastasizing behavior. However, image features such as non-uniform illumination and phase contrast interference rings pose certain difficulties in analyzing these images. We propose a cancer cell classification methodology based on morphological features of 3D phase contrast microscopy and deep neural network with scaled principal component analysis. We initially apply non-uniform illumination correction based on the histogram information of images to correct unstable brightness problems in images and an image intensity-based global thresholding method to compensate for row-contrast artifacts via single-cell detection. We also extracted cross-sections to observe the morphological features using principal component analysis because of the nonsymmetric diffusion pattern of the interference that appeared around each cell. Then, the cell morphologies from an intensity gradient, considering local peaks as bright ring regions, were analyzed. The peak was calculated from the intensity profile from the center point of the cell area, which was the center of the extracted section, to the outer background. Based on the peak information, we extracted representative ten morphological features, applied a min-max scaler to convert the initial features, and used a deep neural network to classify active and inactive cancer cells. The proposed method achieved an area under the receiver operating characteristic curve value of 0.944 and an equal error rate of 0.091. We confirmed that the accuracy of classification using DNN with the proposed method was closer to the results of manual classification by experts, enabling a more precise analysis of cell morphology. This approach improves the accuracy of image-based cellular phenotypic profiling for assessing drug responses in patients.

INDEX TERMS Deep neural network, cancer cell classification, morphological feature extraction, supervised image classification, phase contrast microscopy, principal component analysis.

I. INTRODUCTION

Cancer cells are notorious for their ability to spread to different parts of the body through blood vessels, making tumor treatment challenging [1]. Researchers are actively studying this phenomenon and consider cell shape classification as an effective means of verification [2]. Understanding the shape and morphology of cancer cells is particularly important because their metastasis and migration behaviors are closely tied to these characteristics [2]. Therefore, the ability to analyze and classify cell shapes is recognized as a crucial skill in studying their behavioral patterns.

When conducting research on morphological classification of cells in microscopic images, there are typically three main processes involved: cell segmentation, shape feature extraction, and classifier construction. Cell segmentation,

The associate editor coordinating the review of this manuscript and approving it for publication was Jeon Gwanggil.

which aims to divide the cells for sorting, often utilizes two commonly employed methods: the watershed method and the level-set method [3], [4]. Shape feature extraction methods can be categorized into two types. The first type is based on simple image information, such as Haralick and Zernike moments [5], [6]. The second type combines information from various feature levels. A notable example of the latter is the SLF sets method, which incorporates morphological properties, edge properties, and texture properties [7]. For classifier construction, machine learning techniques like neural networks and Support Vector Machines (SVMs) are predominantly used [8], [9]. These methods enable the creation of classifiers capable of effectively discerning and categorizing different cell shapes.

A cell's phenotype can be influenced by various factors, including epigenetic, genetic, geological, and environmental factors, as well as regulatory rights [10]. Recent studies emphasize the importance of quantitatively analyzing cellular phenotypes using wide-ranging optical imaging techniques. In this regard, the use of transmitted light microscopy allows for the observation of cell morphology without the need for staining, enabling the study of cell changes [11], [12]. However, when observing living cells through 3D reconstruction, a large amount of image data is generated. Manually analyzing such extensive datasets is time-consuming and prone to bias, leading to potentially skewed results [13], [14]. To address this challenge, there is a need for computer-based methods that can accurately recognize and measure individual cell morphological features [15]. In the development of these computational methods, it is crucial to consider common issues encountered in deconvolved images, such as halo artifacts, non-uniform lighting, low cell contrast, and background noise. By addressing these challenges, these methods can be effectively applied in experimental situations involving cells [16].

Previous studies on phase contrast microscopy images have predominantly utilized methods tailored to two-dimensional environments [17], [18], [19]. However, these images present challenges for segmenting individual cells using traditional intensity-based methods, primarily due to non-uniform illumination and halo artifacts. Additionally, common 3D segmentation approaches encounter issues such as light scattering and low contrast, leading to time-consuming and less accurate results. Consequently, an effective cell analysis approach based on image intensity requires a method to identify a focal region where cell morphology is well-defined [15], [20], [21], [22], [23].

In this paper, we propose an effective method for classifying U87 cells using 3D phase contrast microscopy, focusing on their resemblance to glioblastoma multiforme, the most common and lethal brain tumor. Despite being of the same cell type, U87 cells exhibit variations in shape, size, and orientation, posing challenges for accurate classification. The objective of this research is to develop a classifier within a U87 cell sorting framework that can accurately distinguish between active (atypical) and inactive (spherical) cells. To address the difficulties associated with U87 cell classification, we propose a deep neural network-based binary classifier model. This model utilizes morphological characteristics as input information, enabling us to capture cell-specific morphological features that are independent of cell shape, size, and orientation. We evaluate the performance of the proposed classifier by assessing the cancer cell's active/inactive classification accuracy on the cells present in the microscopy images. Through this approach, we aim to improve our understanding of U87 cell behavior and characteristics, ultimately contributing to better insights into glioblastoma multiforme.

The remainder of the paper is organized as follows: In Section II, we introduce the proposed methods, which encompass addressing nonuniform illumination, employing a global segmentation technique, and utilizing a scaled deep neural network (DNN)-based supervised classification method for distinguishing cancer cells into active and inactive categories. The experimental results are presented in Section III. Finally, we provide a comprehensive discussion and draw conclusions based on our findings in Sections IV.

II. RELATED WORK

A. CORRECTING NON-UNIFORM ILLIMINATION

Phase contrast microscopy is widely used to observe live cells. However, it is difficult to analyze the image because the overall brightness and contrast of the image are not constant owing to differences in light absorption and physical properties of the biological gel [20], [21], [22].

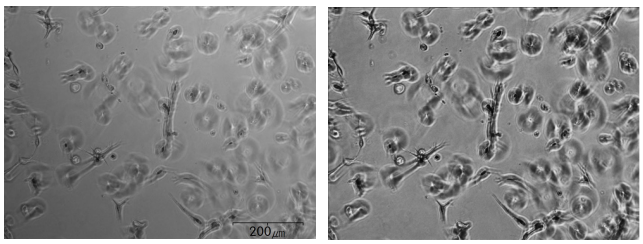

FIGURE 1. Non-uniform illumination correction results (a) Original image (1280 × 1024), (b) Histogram equalization results (1280 × 1024).

Several methods exist for correcting the nonuniform distribution of brightness values in an image according to the lighting location, such as entropy minimization, homomorphic filtering-based methods, and nonuniform illuminance estimation parameters [1]. In this study, we used a modified framework histogram smoothing (MF-HS) algorithm that is robust to over-enhancing problems and can preserve image boundary information, considering the characteristics of phase contrast microscopy [24].

Figure 1 shows the results of applying the MF-HS algorithm. This algorithm solves the problem of nonuniform brightness distribution in the image and improves the problem of low contrast.

B. INDIVIDUAL CELL DETECTION USING HALO PATTERN

A histogram-based global threshold was applied to images corrected for nonuniform illumination to separate the background from the image and detect only the cell regions. We chose the minimum threshold method in a manner similar to the intermodal method. It is iteratively smoothed until only two local maxima remain in the image [25].

A rendering method is required to visualize individual cell detection results in 3D image data. Because rendering is computationally time-consuming, it is generally possible to reduce the computational burden by considering only the region of interest (ROI) of the original image. In this case, only a part of the original image information can be visualized [26]. To compensate for this problem, a high-capacity 3D microscopic image is rendered using a GPU and implemented using texture-based volume rendering and CUDA-accelerated ray casting [26], [27]. Figure 2 shows the results of GPU-based visualization of the detected cells.

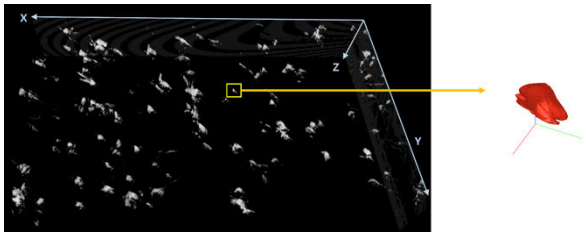

FIGURE 2. 3D visualization of detected cells.

One of the major features of phase contrast microscopy images is the appearance of halo artifacts around the cells. In 3D phase contrast microscopy images, halo patterns appear around cells as bright disks in the XY plane, providing information about out-of-focus phase contrast interference rings as they move away from the cell area when viewed along the z-axis [10] (Figure 3).

Each cell in a 3D phase contrast microscopy image has a different optimal focus plane depending on the direction of movement. Consequently, the accuracy of analysis results using general 2D surfaces is limited. To estimate the direction of each cell and extract a well-focused diffusion surface, the first principal axis vector is calculated using the distribution of pixels existing in the initial area of each cell and the first principal axis, which is the cross-section intersecting the center of each cell and extracting a meaningful cross-section through the center of mass of the passing region. To this end, principal component analysis (PCA) [28] was used to clearly represent the halo pattern around each cell (Figure 4) [21], [29], [30].

Passing through the center of mass of the detected individual cell area and considering the halo pattern information in the cross-section perpendicular to the first principal axis [20], only the cell area was extracted through the active contour method with the center point as the seed point. The remaining area was designated as the background area as shown in Figure 5. In this manner, the cell area was segmented using

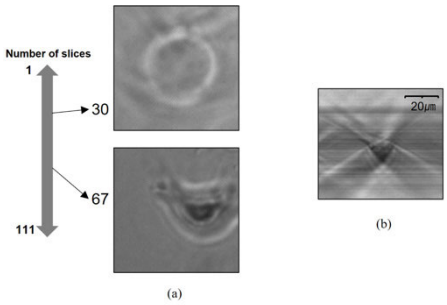

FIGURE 3. Cell appearance correlation. (a) XY plane, (b) XZ plane.

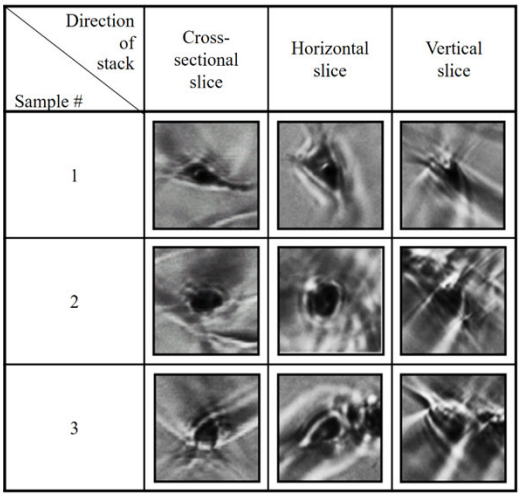

FIGURE 4. Comparison of cells according to each plane.

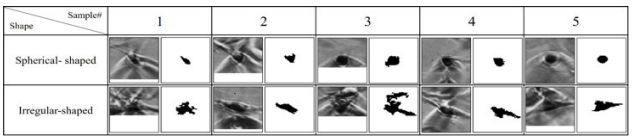

FIGURE 5. Cell appearance correlation. (a) XY plane, (b) XZ plane.

intensity-based information, considering the characteristics of the image. In the next section, we used the segmented region information to extract the features.

III. PROPOSED METHOD

Figure 6 shows an overall flowchart of the proposed classification method. In this study, we propose a method for classifying cells according to their morphological characteristics after dividing them into individual cells based on the characteristics of 3D phase contrast microscopy images. The proposed method consists of three modules such as image processing, model training and model testing. In the image processing module, living U87 glioblastoma cells were collected and dispersed in a 3D cell matrix in a Matrigel environment. Using a phase contrast microscope, the cells were imaged at 10× magnification with a z-step distance of 5μm. We applied image restoration technique based on

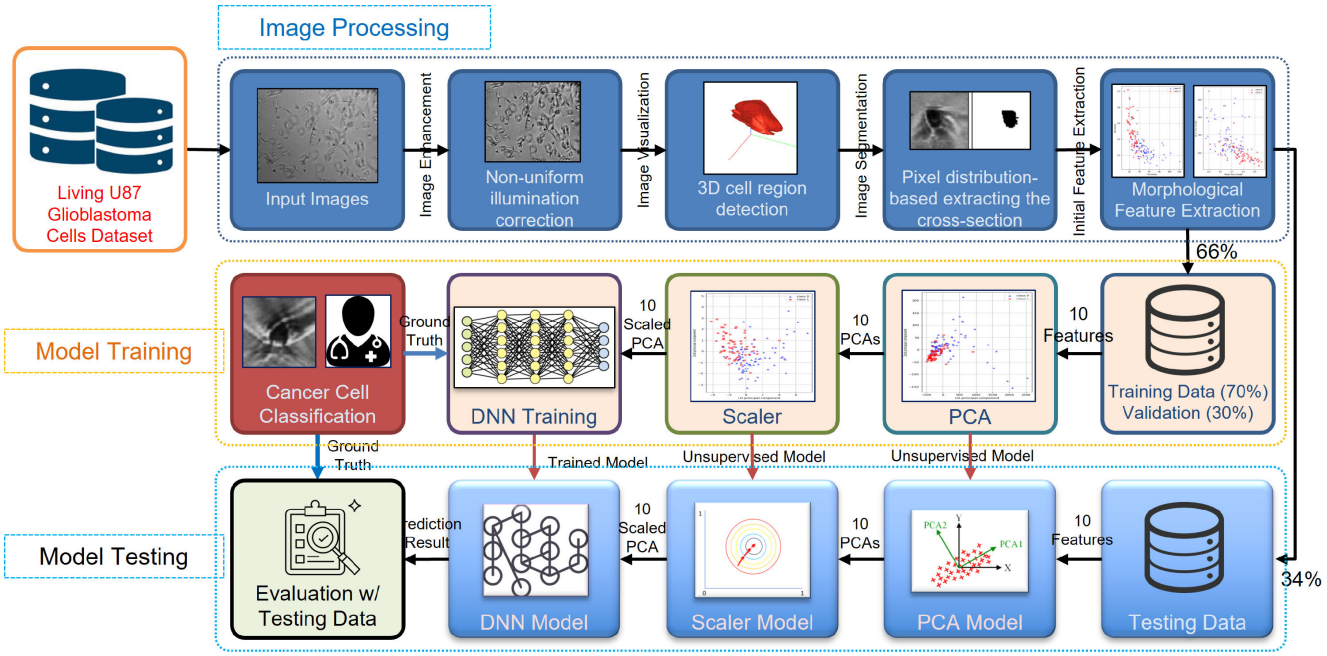

FIGURE 6. The overview of the proposed methodology.

non-uniform illumination correction, visualized the enhanced images using 3D cell region detection and applied image segmentation using pixel distribution based extracting the cross-section. Ten morphological features from each binary cell image are extracted and a deep neural network method with a scaled PCA for accurate classification is applied in model training and testing modules. First, the preprocessed U87 dataset for ten input feature variables from 224 cell image samples was used to train (66%) and test (34%) the models. Thirty percent of the training samples was used to validate the training process. Second, the morphological feature variables were converted to principal components (PCs) based on scalers, such as min-max, standard, quantile, and no scaler, using PCA. Third, we trained the deep neural network (DNN) model using the preprocessed variables and evaluated its predictive performance with annotations labeled by a cell classification expert. To evaluate the accuracy of the test results, the data for the test models were completely separated from the training data used for testing.

A. MORPHOLOGICAL FEATURE EXTRACTION

The characteristics of the segmented cell area were extracted to determine the degree of activation of the U87 cells. The extracted features are as follows: First, we extracted the x- and y-coordinates of the centroids, which represented the centroid position information on 3D Matrigel. The area of the cell region was extracted from the actual number of pixels in the region. In addition, to obtain a result that excluded weak noise, the area of the polygon acquired through the convex hull was calculated. The perimeter distance around the boundary of the region was extracted to obtain additional size information. In addition, various morphological features were extracted to classify the spherical shapes by considering the influence of halo artifact interference around the extracted area. First, we calculated the circularity for the roundness extraction of the cell area. Then, the ellipse that has the same second moment as the region computes the eccentricity, and the ratio of the pixels in the convex hull that are also in the region computes the solidity. It also computes the diameter of a circle with the same area as the region (Equiv Diameter) and the length of the major and minor axes of the ellipse that has the same normalized second central moments as the region. Among the extracted features, Figure 7 shows the selected significant features in 2D plots.

As shown in Figure 7 (a) and (b), among the ten feature variables, the discrimination of the Major and Minor Axis Lengths, Circularity, and Perimeter variables was relatively good. The remaining feature variables, including those in Figure 7(c) and (d), were relatively low compared to the four main variables.

B. CLASSIFICATION

Based on the binary images obtained after the threshold-based process, we propose a deep neural network method with a scaled PCA for accurate classification. In the proposed methodology, we extracted 10 morphological features from each binary cell image: area, centroid X, centroid Y, circularity, eccentricity, equivalent diameter, perimeter, solidity, major axis length, and minor axis length. We utilized a simple feedforward neural network and backpropagation algorithm to train the proposed model, optimizing diverse combinations of hyperparameters, including the activation function,

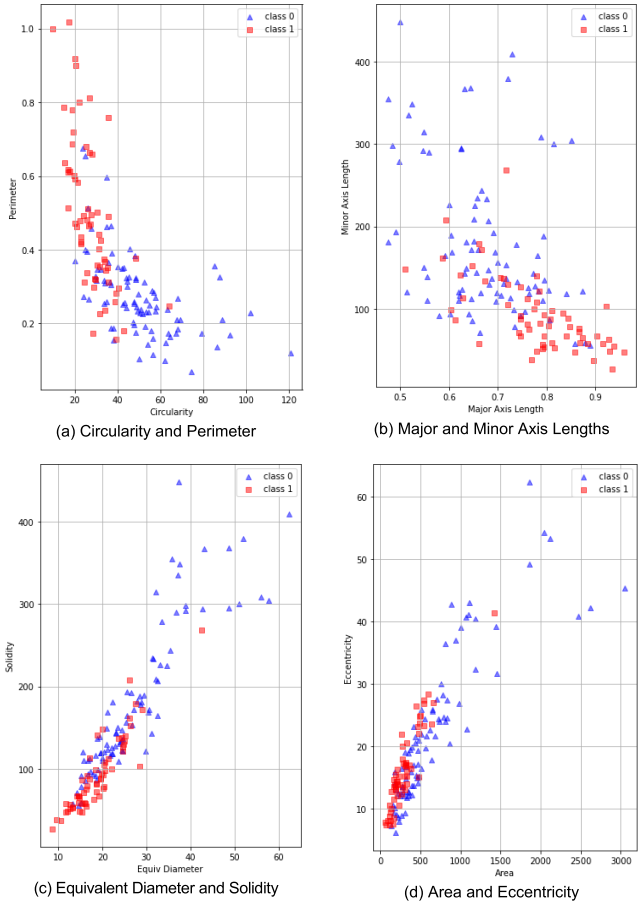

FIGURE 7. Diverse feature variables: class 0 is normal cell images (blue triangle) and class 1 is cancer cell images (red rectangular).

regularization technique, number of hidden layers, and number of neurons in each layer. The best-performing network architecture included four hidden layers, with the first three containing 200 neurons and the last hidden layer containing 10 neurons. The last layer has two neurons and produces regression outputs. To prevent overfitting and ensure stable convergence, 2 batch normalization [31] and dropout [32] techniques were applied to the first three hidden layers, whereas the ReLU activation function [33] was used in all the hidden layers and the output layer. They also used Adam optimization [34] with a binary cross-entropy loss function and a learning rate of 0.001 for the training process. A detailed description of the DNN architecture is presented in Figure 8. We systematically optimized the hyperparameters and utilized various techniques to enhance the robustness of the model and prevent overfitting.

C. HYPERPARAMETER TUNING

The training environment for DNNs involves several hyperparameters that must be optimized to achieve the best possible performance. We fine-tuned the hyperparameters, such as the depth of the DNN and number of nodes, to create an optimal model that improves the prediction performance.

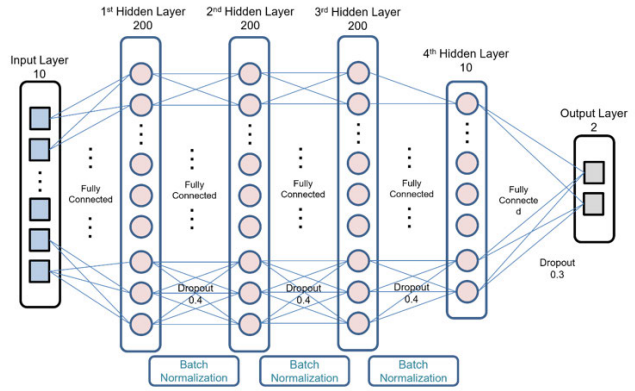

FIGURE 8. The architecture of the proposed DNN.

Because there are no general rules for tuning the hyperparameters, we used a trial-and-error approach to train models with 2–8 layers and 10–250 nodes. We also employed two techniques to address overfitting: dropout and batch normalization. Dropout works by randomly weighting the outputs of nodes to prevent the model from overemphasizing specific nodes. Batch normalization ensures that the initial weights are appropriate for the feed-forward data, which helps prevent data loss. We used a range of dropout values (0.1 to 0.5) and chose the optimal value of 0.4 based on testing results. Overall, our systematic approach to fine-tuning hyperparameters and use of appropriate techniques led to the development of an effective DNN model for specific tasks.

IV. RESULTS AND DISCUSSION

A. PERFORMANCE METRICS

Five common quality metrics were considered, including sensitivity (*Sn.*), Specificity (*Sp.*), positive predictive value (*PP.*), accuracy (*Acc.*), Equal Error Rate (*EER*) and area under the ROC curve (*AUC*). AUC was used for the initial performance evaluation for a better comparison based on only one performance metric because, as indicated by Bradley [35], accuracy cannot explain the measure for sparse (imbalanced) datasets. AUC can also be used to evaluate the overall performance using a single performance metric without requiring a threshold for the probabilities calculated from the classification algorithms.

$$Sn. = TP/(TP + FN) \quad (1)$$

$$Sp. = TN/(TN + FP) \quad (2)$$

$$PP. = TP/(TP + FP) \quad (3)$$

$$Acc. = (TP + TN)/(TP + FN + FP + TN) \quad (4)$$

B. PERFORMCE COMPARISON

PCA with the scaler preprocessed all input data to generate new 10 variables to change the scales and variances. The combinations of PCs of the four different PCAs (1st and 2nd PCs) are shown in Figure 9: (a) PCAs with Min Max scaler, (b) PCAs with Standard scaler, (c) PCAs with

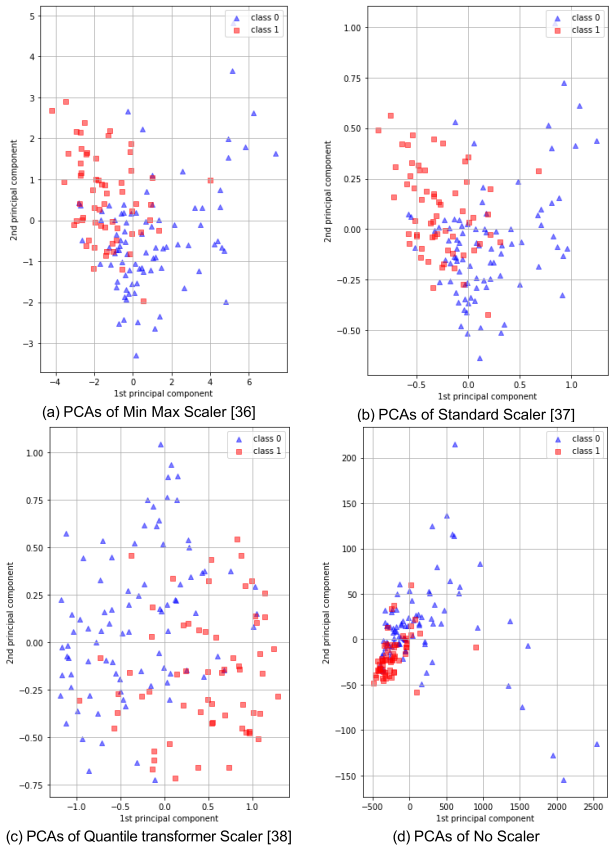

FIGURE 9. Diverse Feature scaling plots with the PCA: class 0 is normal cell images (blue triangle) and class 1 is cancer cell images (red rectangular).

Quantile scaler, and (d) PCAs without the scaler. As can be seen in Figure 9(a), the active cancer cell data (red boxes) are gathered on one side, making it possible to see that the min/max method provides meaningful feature values compared to other combinations. In addition, according to the test results in Table 1, a DNN with a PCA min/max scaler shows the best mixture.

To verify the performance of preprocessing related to PCA and different scalers, we compared the results using one performance metric: the AUC or EER values. Table 2 compares the overall performance using either AUCs or EERs from different combinations of PCAs and scalers. The best AUC performances (0.944 and 0.935, marked in bold) were obtained by the DNN with a PCA-min-max scaler or the DNN with a PCA-standard scaler, followed by the SVC with a PCA-min-max scaler. In terms of EERs, the best EER performances were the DNN with a min-max or quantile transform scalers, marked in bold in Table 1.

According to the AUC and EEG results, the min-max scaled PCA with most classifiers showed relatively better performance than other scalers in terms of AUC values. Table 2 summarizes the performance characteristics of the five classification algorithms with minimum-maximum scaled PCA for classifying images as cancer cells for the given testing data. The optimal threshold for classifying cancer cells was 0.5, based on all model parameters, resulting in an Acc of 89.61% for Sn. of 84.85%, Sp. of 93.18%, and PP. of 90.32%. For comparison, we also report the performance of PCA without a scaler. All thresholds of the compared classifiers were adjusted to balance the sensitivity and specificity values. The proposed scaled PCA/DNN method produces the best results, followed by the SVC method. Based on the comparative results, we conclude that the scaled PCA/DNN method outperformed the other classifiers in terms of all performance metrics.

C. SIGNIFICANCES OF THE PROPOSED METHOD

There are several significances in this study. First, comparing to the traditional H&E staining performed in clinical pathology for tumor grading, it is important to classify the live cells because it will be possible to observe how activity varies over time and how location changes using living cells later. Second, it is expected that the analysis method presented in this paper can be extended to other types of cancer cells. Third, although actual patient-derived cell images could provide more information compared with a single replicate of

TABLE 1. Comparison of AUC and EER results.

(A) AUC

AUC	Min-Max	Standard	Quantile	No Scaler
DNN	**0.944**	**0.937**	0.925	0.89
RF	0.867	0.857	0.846	0.896
ABC	0.909	0.875	0.844	0.87
GNB	0.894	0.896	0.923	0.943
SVC	0.935	0.933	0.918	0.842

(B) EER

EER	Min-Max	Standard	Quantile	No Scaler
DNN	**0.091**	**0.159**	0.091	0.205
RF	0.205	0.227	0.182	0.182
ABC	0.159	0.182	0.205	0.136
GNB	0.182	0.159	**0.159**	**0.114**
SVC	0.182	0.159	**0.159**	**0.273**

* Min-max (Min-Max scaler [36]), Standard (Standard Scaler [37]), Quantile (Quantile Transformer Scaler [38])

TABLE 2. Comparison of the Proposed DNN models with Min-max Scaler and other methods.

Scaler	Model	*TP*	*FP*	*FN*	*TN*	*Sn.*	*Sp.*	*PP*	*Acc*	*AUC*
Min-Max	DNN	28	3	5	41	**84.85**	**93.18**	**90.32**	**89.61**	**0.944**
No Scaler	DNN	28	12	5	32	84.85	72.73	70.00	77.92	0.859
Min-Max	ABC	27	5	6	39	81.82	88.64	84.38	85.71	0.909
	RF	24	7	9	37	72.73	84.09	77.42	79.22	0.867
	GNB	25	8	8	36	75.76	81.82	75.76	79.92	0.894
	SVC	28	4	5	40	84.85	90.91	87.50	88.31	**0.935**

cell culture, the proposed method including scaled PCA with deep neural network shows robust result (AUC of 0.944) even with a single replicate of cell culture.

The step distance refers to the intervals between focus levels or positioning adjustments in a microscope and acts as a significant role when creating 3D reconstructions or analyzing fine structures in detail. The step distance used in this study is $5\mu m$ with 10x magnification of 3D phase contrast microscopy. When capturing images at different depths, especially in detailed studies covering layers or depths, the step distance is significant. The step distance determines how finely the microscope can focus on different depths of the sample. The smaller step distance the more detailed and higher resolution imaging. This allows the microscope to capture more images at closer intervals, resulting in a clearer and more continuous depiction of the structure of the sample.

V. CONCLUSION

In this study, we proposed a method for classifying the morphology of active/inactive cancer cells based on scaled PCA and DNN. Using the morphological features extracted from microscopic images, a classification accuracy of 94% was obtained, which is better than the previous SVM-based classification results. Consequently, it was quantitatively confirmed that the accuracy of classification using DNN with the proposed method was closer to the results of manual classification by experts, enabling a more precise analysis of cell morphology. To improve the accuracy of the morphological classification of cancer cells, image processing was performed by reflecting the 3D phase contrast microscopic image characteristics, and cell feature information was extracted. This procedure allowed for accurate analysis of cell morphology. This approach improves the accuracy of image-based cellular phenotypic profiling for assessing drug responses in patients.

VI. LIMITATION AND FUTURE WORK

While this study has provided valuable insights into cancer cell classification based on morphological features of 3D phase contrast microscopy images, several limitations should be considered, including the limited number of cell-based testing and focusing only on static cell images. To address these limitations and further explore this area, future research could focus on incorporating more cell-based testing to ensure statistical consistency in our future research. Additionally, we will explore extracting more information from phase contrast imaging to enhance our analysis. In terms of live cells, we will analyze the spatial movement of active and inactive cells using the images captured at 0 hours, 11 hours, and 25 hours from the dataset used in this study.

ACKNOWLEDGMENT

The authors would like to thank Dr. Wong of The Methodist Hospital Research Institute (TMHRI) for providing 3D phase contrast microscopic images of U87 cells.

REFERENCES

[1] S. Wadler, H. Zhang, M. Cammer, and X.-P. Hu, "Quantification of ribonucleotide reductase expression in wild-type and hydroxyurea-resistant cell lines employingin SituReverse transcriptase polymerase chain reaction and a computerized image analysis system," *Anal. Biochemistry*, vol. 267, no. 1, pp. 24–29, Feb. 1999.

[2] Y. Hamamoto, S. Uchimura, and S. Tomita, "On the behavior of artificial neural network classifiers in high-dimensional spaces," *IEEE Trans. Pattern Anal. Mach. Intell.*, vol. 18, no. 5, pp. 571–574, May 1996.

[3] N. N. Kachouie, P. Fieguth, and E. Jervis, "Watershed deconvolution for cell segmentation," in *Proc. 30th Annu. Int. Conf. IEEE Eng. Med. Biol. Soc.*, Aug. 2008, pp. 375–378.

[4] Y. Zhou, A. Kuijper, and L. He, "Multiphase level set method and its application in cell segmentation," in *Proc. 5th IASTED Int. Conf. Signal Process., Pattern Recognit. Appl.*, 2008, pp. 134–139.

[5] K. Huang and R. F. Murphy, "Automated classification of subcellular patterns in multicell images without segmentation into single cells," in *Proc. 2nd IEEE Int. Symp. Biomed. Imag., Macro Nano*, vol. 2, Apr. 2004, pp. 1139–1142.

[6] N. A. Hamilton, R. S. Pantelic, K. Hanson, and R. D. Teasdale, "Fast automated cell phenotype image classification," *BMC Bioinf.*, vol. 8, no. 1, pp. 1–8, Dec. 2007.

[7] X. Chen and R. F. Murphy, "Objective clustering of proteins based on subcellular location patterns," *BioMed Res. Int.*, vol. 2005, no. 2, pp. 87–95, Jan. 2005.

[8] M. A. Arbib, *Brain Theory and Neural Networks*. Cambridge, MA, USA: MIT Press, 1995.

[9] V. N. Vapnik, *The Nature of Statistical Learning Theory*. Cham, Switzerland: Springer, 1995.

[10] D. J. Wooten and V. Quaranta, "Mathematical models of cell phenotype regulation and reprogramming: Make cancer cells sensitive again!" *Biochimica et Biophysica Acta (BBA)-Rev. Cancer*, vol. 1867, no. 2, pp. 167–175, Apr. 2017.

[11] P. Friedl, K. S. Zänker, and E.-B. Bröcker, "Cell migration strategies in 3-D extracellular matrix: Differences in morphology, cell matrix interactions, and integrin function," *Microsc. Res. Technique*, vol. 43, no. 5, pp. 369–378, Dec. 1998.

[12] K. Li, E. D. Miller, M. Chen, T. Kanade, L. E. Weiss, and P. G. Campbell, "Cell population tracking and lineage construction with spatiotemporal context," *Med. Image Anal.*, vol. 12, no. 5, pp. 546–566, Oct. 2008.

[13] G. Danuser, "Computer vision in cell biology," *Cell*, vol. 147, no. 5, pp. 973–978, Nov. 2011.

[14] G. Ye and M. Kaya, "Automated cell foreground–background segmentation with phase-contrast microscopy images: An alternative to machine learning segmentation methods with small-scale data," *Bioengineering*, vol. 9, no. 2, p. 81, Feb. 2022.

[15] H. Su, Z. Yin, S. Huh, and T. Kanade, "Cell segmentation in phase contrast microscopy images via semi-supervised classification over optics-related features," *Med. Image Anal.*, vol. 17, no. 7, pp. 746–765, Oct. 2013.

[16] C. Decaestecker, O. Debeir, P. Van Ham, and R. Kiss, "Can anti-migratory drugs be screened in vitro? A review of 2D and 3D assays for the quantitative analysis of cell migration," *Medicinal Res. Rev.*, vol. 27, no. 2, pp. 149–176, Mar. 2007.

[17] J. Pan, T. Kanade, and M. Chen, "Learning to detect different types of cells under phase contrast microscopy," in *Proc. Microscopic Image Anal. Appl. Biol. (MIAAB)*, 2009, pp. 1–34.

[18] S. Sakuma and T. Tanaka, "Cell tracking algorithm using the phase contrast microscopy image," in *Proc. SICE Annu. Conf. (SICE)*, Akita, Japan, 2012, pp. 1926–1929.

[19] J. Orikawa and T. Tanaka, "Cell segmentation from phase-contrast images using hybrid watershed and region growing algorithm for genomic drug discovery," in *Proc. SICE Annu. Conf.*, Aug. 2010, pp. 84–88.

[20] M. S. Kang, S. M. Song, H. Lee, and M. H. Kim, "Cell morphology classification in phase contrast microscopy image reducing halo artifact," *Proc. SPIE*, vol. 8227, pp. 260–268, Feb. 2012.

[21] M.-S. Kang, J.-E. Lee, H.-R. Kim, and M.-H. Kim, "Classification of tumor cells in phase-contrast microscopy image using Fourier descriptor," *J. Biomed. Eng. Res.*, vol. 33, no. 4, pp. 169–176, Dec. 2012.

[22] M. S. Kang, H. R. Kim, and M. H. Kim, "Cell classification in 3D phase-contrast microscopy images via self-organizing maps," in *Proc. 10th ISVC*, Las Vegas, NV, USA. Cham, Switzerland: Springer, 2014, pp. 652–661.

[23] H. Lee and J. Kim, "Retrospective correction of nonuniform illumination on bi-level images," *Opt. Exp.*, vol. 17, no. 26, p. 23880, 2009.

[24] T. Arici, S. Dikbas, and Y. Altunbasak, "A histogram modification framework and its application for image contrast enhancement," *IEEE Trans. Image Process.*, vol. 18, no. 9, pp. 1921–1935, Sep. 2009.
[25] J. M. S. Prewitt and M. L. Mendelsohn, "The analysis of cell images," *Ann. New York Acad. Sci.*, vol. 128, no. 3, pp. 1035–1053, 1966.
[26] M. S. Kang, J. E. Lee, W. Jeon, H. K. Choi, and M. H. Kim, "Intensity-based segmentation and visualization of cells in 3D microscopic images using the GPU," *Proc. SPIE*, vol. 8589, pp. 27–34, Feb. 2013.
[27] A. Appel, "Some techniques for shading machine renderings of solids," in *Proc. AFIPS*, 1968, pp. 37–45.
[28] L. I. Smith et al., *A Tutorial on Principal Components Analysis*, Ithaca, NY, USA, Feb. 2002. [Online]. Available: http://kybele.psych.cornell.edu/~/Psych-465-Spring-2003/PCA-tutorial.pdf
[29] Y. Watanabe, "A method for volume estimation by using vector areas and centroids of serial cross sections," *IEEE Trans. Biomed. Eng.*, vols. BME–29, no. 3, pp. 202–205, Mar. 1982.
[30] J. Shlens, "A tutorial on principal component analysis," 2014, *arXiv:1404.1100*.
[31] S. Ioffe and C. Szegedy, "Batch normalization: Accelerating deep network training by reducing internal covariate shift," in *Proc. Int. Conf. Mach. Learn.*, 2015, pp. 448–456.
[32] N. Srivastava, G. Hinton, A. Krizhevsky, I. Sutskever, and R. Salakhutdinov, "Dropout: A simple way to prevent neural networks from overfitting," *J. Mach. Learn. Res.*, vol. 15, no. 1, pp. 1929–1958, 2014.
[33] K. He, X. Zhang, S. Ren, and J. Sun, "Delving deep into rectifiers: Surpassing human-level performance on ImageNet classification," in *Proc. IEEE Int. Conf. Comput. Vis. (ICCV)*, Dec. 2015, pp. 1026–1034.
[34] D. P. Kingma and J. Ba, "Adam: A method for stochastic optimization," 2014, *arXiv:1412.6980*.
[35] A. P. Bradley, "The use of the area under the ROC curve in the evaluation of machine learning algorithms," *Pattern Recognit.*, vol. 30, no. 7, pp. 1145–1159, Jul. 1997.
[36] *MinMaxScaler*. Accessed: Feb. 21, 2025. [Online]. Available: https://scikit-learn.org/stable/modules/generated/sklearn.preprocessing.MinMaxScaler.html
[37] *StandardScaler*. Accessed: Feb. 21, 2025. [Online]. Available: https://scikit-learn.org/stable/modules/generated/sklearn.preprocessing.StandardScaler.html#sklearn.preprocessing.StandardScaler
[38] *QuantileTransformer*. Accessed: Feb. 21, 2025. [Online]. Available: https://scikit-learn.org/stable/modules/generated/sklearn.preprocessing.QuantileTransformer.html#sklearn.preprocessing.QuantileTransformer

MISUN KANG received the B.S., M.S., and Ph.D. degrees in computer science and engineering from Ewha Womans University, Seoul, South Korea, in 2007, 2012, and 2017, respectively. She was Research Fellow with the Department of Computer Science and Engineering, Ewha Womans University. She was a Staff Engineer with Samsung Display. She is currently an Assistant Professor with the Department of Applied Intelligence, Hansung University. Her research interest includes AI-based bio-medical image processing.

JUNGYOON KIM received the B.S. degree in electronics and the M.S. degree in electrical and computer engineering from the University of Ulsan, South Korea, in 2004 and 2006, respectively, and the Ph.D. degree in information sciences and technology from The Pennsylvania State University, University Park, PA, USA, in 2014. He is currently an Assistant Professor in computer science with Kent State University, where he is also the Founding Director of the Smart Communities and IoT Laboratory. His areas of experience and expertise are in smart health and wellbeing, especially in real-time cardiovascular disease and stress monitoring, physiological sensor design, and intelligent analytics for decision supports; environmental monitoring and assessment—especially in air quality monitoring and cut slope movement monitoring and ubiquitous computing—especially in embedded system design, energy efficient processing, and programming model for networking performance.